

A new seismic tomography system for geotechnical centrifuges

Khader Ibrahim Rammah^{1#} , Mostafa Ali Ismail¹ , Jesse Costa² ,

Mario Vicente Riccio Filho³ 

Article

Keywords

Seismic tomography
Shear-wave velocity
Bender elements
Inversion
Travel-time
Centrifuge testing

Abstract

Seismic tomography has been extensively used in geophysics for different purposes, including geological mapping, characterisation of inner earth structure and prospecting for oil and gas. In geophysics, seismic or electromagnetic waves are commonly used to provide tomographic information. In the geotechnical area, seismic tomography is emerging as a promising technique that can be used to determine the spatial variability of shear wave velocities and hence the small strain stiffness of geomaterials, especially when used in the centrifuge where in-situ stress conditions can be mimicked closely. This paper describes the development of a seismic tomography technique in the centrifuge. This technology can be used to image variations of soil stiffness under various mechanical, chemical and physical conditions. The paper describes the various components of the system, which includes arrays of small-size bender elements, hardware and software used to transmit, receive and acquire the shear wave signals during a centrifuge test. The paper illustrates the performance of the system at both 1g and in the centrifuge. Results of tomographic inversion performed on travel-time data obtained from these tests are discussed.

1. Introduction

Tomography is a well-known technique used in many branches of science to create images of projections ('tomograms') of hidden objects by inverting boundary measurements of chemical, electrical, thermal or mechanical parameters. The technique is extensively applied in inverting X-ray measurements (X-ray tomography) in medicine. In other fields of science, such as geophysics, oil and gas exploration, and geotechnical field testing, seismic or electromagnetic waves are used as a tomographic measurement. This type of tomography is known as 'seismic tomography' or ST. During the past few decades, the use of seismic tomography has become more common in earth sciences for the purpose of both compression and shear wave velocity imaging in the area of geophysics, geotechnics and oil and gas exploration (Woodward et al., 2008).

In seismic tomography, the technique commonly refers to the measurement of arrival times of either compression or shear waves that propagate through the subsurface medium. The arrival time of a propagating wave depends on the properties of the medium through which the wave propagates, such as the compression and shear moduli of the soil (Menke, 1984; Young et al., 1988).

In geotechnical engineering, seismic methods can be an excellent diagnostic tool for soil characterisation since wave propagation characteristics can be directly related to geotechnical parameters, such as the elastic moduli at small strains. The majority of geotechnical projects nowadays require the determination of the shear stiffness at small strains, G_0 , which is an essential parameter for many geotechnical applications, including the evaluation of deformations around geotechnical structures and the prediction of dynamic/earthquake response (Pennington et al., 2001; Rammah et al., 2004).

Centrifuge testing has become a routine experimental method in both onshore and offshore geotechnical engineering. Therefore, it is crucial to characterise soil models in terms of G_0 during flight. This requires a system for propagating shear waves within the soil body and receivers to pick up the arrival of the shear waves. Several of these components can enable ST to be performed on centrifuge soil models.

A literature review has revealed that few attempts have been made to perform seismic measurements in a geotechnical centrifuge or even 1g models. An attempt was made by Ismail & Hourani (2003) for a simple 1g model in an acrylic cylinder filled with clay. A centrifuge system was described by Fu et al. (2004), where shear waves were generated through sand samples during centrifuge experiments. In their system, the shear waves were generated by a series

¹The University of Western Australia, School of Civil Engineering, Perth, Western Australia, Australia.

²Universidade Federal do Pará, Faculdade de Geofísica, Belém, PA, Brasil.

³Universidade Federal de Juiz de Fora, Programa de Pós-graduação em Engenharia, Juiz de Fora, MG, Brasil.

#Corresponding author. E-mail address: khader.rammah@gmail.com

Submitted on January 23, 2022; Final Acceptance on October 26, 2022; Discussion open until May 31, 2023.

<https://doi.org/10.28927/SR.2023.000922>



This is an Open Access article distributed under the terms of the Creative Commons Attribution License, which permits unrestricted use, distribution, and reproduction in any medium, provided the original work is properly cited.

of three pairs (transmitter and receiver) of bender element transducers installed at different depths in the soil model. Earlier, Kita et al. (1992) measured the shear wave velocity of sand in a centrifuge model. Recently, a small-scale shear wave tomography device was built by Lee et al. (2005) for geotechnical application. They used mainly an array of bender elements as sources and receivers to scan a soil body in a box under 1g conditions.

The literature has shown that no attempt has been made to build a complete ST facility with high resolution for routine use in centrifuge modelling. Such a powerful facility can help better understand soil behaviour by providing a complete picture of the spatial variation of the shear wave velocity under general stress, chemical and/or physical conditions.

In the present research, a high-resolution ST system has been developed for the geotechnical centrifuge at the University of Western Australia (UWA). This system was used to image the variation of shear wave velocity (and hence soil stiffness) for different soil models in the centrifuge. A brief description of the development has already been published (Rammah et al., 2006). The present paper describes the system components in detail, emphasising its performance. Critical issues relating to the selection of transducers and their performance and the resolution of the resulting tomographic images are discussed. The paper presents some of the results of tomographic inversion of travel-time data obtained from 1g and centrifuge tests.

2. Design requirements for centrifuge ST system

Design criteria for tomographic studies can be found in the geophysics literature (Nolet, 1987; Santamarina & Fratta, 1998; Berryman, 1991). In addition, a study relevant to geotomography (seismic tomography applied in geotechnical engineering) addressing the design criteria was carried out by Fernandez & Santamarina (2002).

2.1 Fundamentals of a tomographic experiment

The most common configuration in a tomographic experiment is cross-hole tomography, shown in Figure 1a. The aim of a tomographic experiment is to image the medium between the two boreholes depicted and collect data relevant to the unknown parameters. For this purpose, the medium is discretised into a mesh of n pixels (or cells), as shown in Figure 1b and Figure 1c. The number of measurements m is equal to the number of rays between the sources and receivers (i.e., m is a function of the number of sources and receivers).

For a single ray path, the travel time along the ray AB in Figure 1c is given in Equation 1:

$$t = \int_A^B \left(\frac{1}{V} \right) dl \quad (1)$$

where A and B are the source (transmitter) and receiver positions, V is the wave velocity, and dl is an increment of length along the arc between the two (in this case, it is considered a straight line). Equation 1 can be rewritten in a summation form given in Equation 2:

$$t_i = \sum_{j=1}^n \left[\frac{L_{ij}}{V_j} \right] \quad (2)$$

where t_i is the travel time along the i -th ray (Figure 1c), L_{ij} is the travel distance or length travelled by the i -th ray in each j -th cell (pixel) at velocity V_j as presented in Figure 1d, and n is the number of cells the i -th ray intersects.

For all the rays (m rays), Equation 2 can be written in a matrix form as presented in Equation 3:

$$[T] = [L].[S] \quad (3)$$

where $[T]$ is the travel time vector (dimensions $m \times 1$), which is formed by all the measurements in the tomographic experiment, $[L]$ is the matrix of travel lengths (dimensions $m \times n$) obtained from the geometry of the model (i.e., the mesh shown in Figure 1, and $[S]$ is the slowness vector for all the pixels in the mesh (dimension $n \times 1$). In geophysics, it is common to address a medium with its slowness values. The slowness is the reciprocal of the velocity as expressed in Equation 4:

$$S = \frac{1}{V} \quad (4)$$

A tomographic experiment involves the determination of the slowness matrix, and hence velocity, by carrying out an inversion procedure for the linear system given in Equation 3.

The number of pixels, N_p , representing the unknown region between the two boreholes in Figure 1 depends on the number of transducers in the vertical dimension and the separation distance between the two boreholes L_b . This can be written in Equation 5:

$$N_p = \text{Integer} \left(\frac{H}{\Delta z} + 0.5 \right) \cdot \text{Integer} \left(\frac{L_b}{\Delta z} + 0.5 \right) \quad (5)$$

where Δz is the vertical separation distance between transducers, and H is the depth of the borehole. The above equation implies that the higher the number of transducers, the smaller the separation distance and the higher the number of pixels. Therefore, a higher resolution implies a smaller pixel size, which can be achieved by increasing the number of pixels.

As mentioned before, the tomographic inversion aims to determine the velocity (or slowness) in each pixel, and, therefore, the number of unknowns in the tomographic inversion process equals the number of cells. This is valid only in the case of an isotropic medium, where each cell is represented by invariant velocity. However, the number of

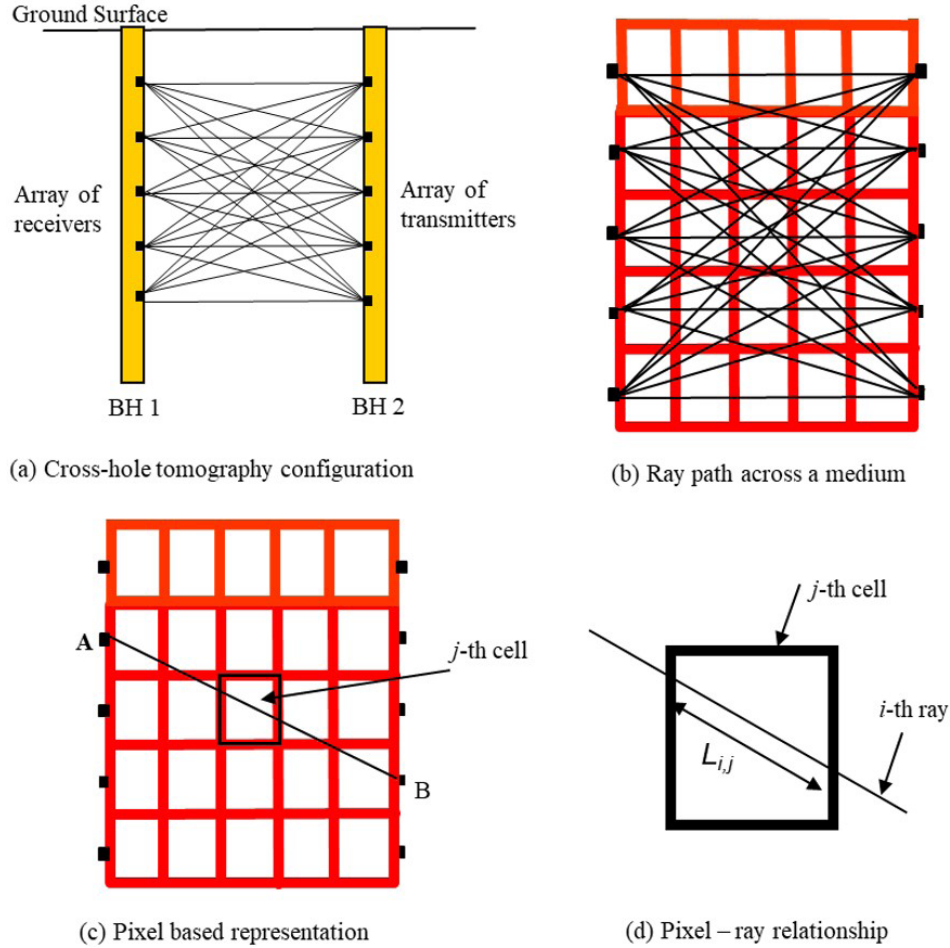


Figure 1. Model representation in cross-hole tomography.

unknowns will increase if anisotropy is considered. In elliptical anisotropy (where the wavefront travels in an elliptic shape), each cell is represented by two perpendicular components of unknown slowness.

The number of measurements, m , in cross-hole tomographic configuration is equal to the number of sources times the number of receivers, as expressed in Equation 6:

$$m = \left[\text{Integer} \left(\frac{H}{\Delta z} + 0.5 \right) \right]^2 \quad (6)$$

Ideally, a well-determined problem is obtained when the number of measurements equals the number of unknowns, and in this case, the solution would be exact. However, this is not always the case, as sometimes the number of measurements is higher than the number of unknowns, which yields an “over-determined problem”. Ill-conditioned problems occur if the number of measurements is less than the number of unknowns. In most cases in cross-hole tomography, some pixels do not have enough information (i.e. insufficient number of rays crossing them), such as those pixels at the

top and bottom regions in Figure 1b. This normally results in a case called a “mixed-determined” problem.

A solution to overcome an ill-conditioned problem is to increase the number of measurements. This can be achieved by increasing the rays covering (or the spatial coverage) the unknown region (Berryman, 1991).

3. Determination of the resolution of a tomographic image

As indicated, better tomography resolution can be achieved by decreasing the vertical distance between the wave transducers Δz . However, as explained below, theoretical and practical restrictions may limit the minimum separation between successive transducers.

3.1 Wavelength

The wavelength λ defines the maximum resolution that can possibly be achieved by tomography. In general, it is not feasible to detect anomalies or variations that are smaller than one wavelength (Berryman, 1991). The wavelength is,

in turn, dependent on the velocity V of the scanned medium as well as the transmitted wave frequency f (it should be noted that frequency should be selected such that the wave can be felt clearly by the receivers before it attenuates due to the geometry and the material damping). Equation 7 links all these three quantities:

$$\lambda = \frac{V}{f} \quad (7)$$

3.2 Fresnel ellipse criterion

Fresnel ellipse provides a criterion for the optimal separation between transducers below which the resolution does not improve. Such optimisation reduces both cost and time. To avoid redundancy, the separation of the transducers should conform to the criterion of Fresnel's ellipse (according to Fresnel's principle, each ray has an elliptical zone). In order to avoid any redundant measurements, the transducer's separation Δz has to be chosen in a way to avoid any intersection between these ellipses and yet leaving no regions uncovered. The size of Fresnel's ellipse in Figure 2 is estimated in Equation 8:

$$(L_1 + L_2) \leq (L_b + \frac{\lambda}{2}) \quad (8)$$

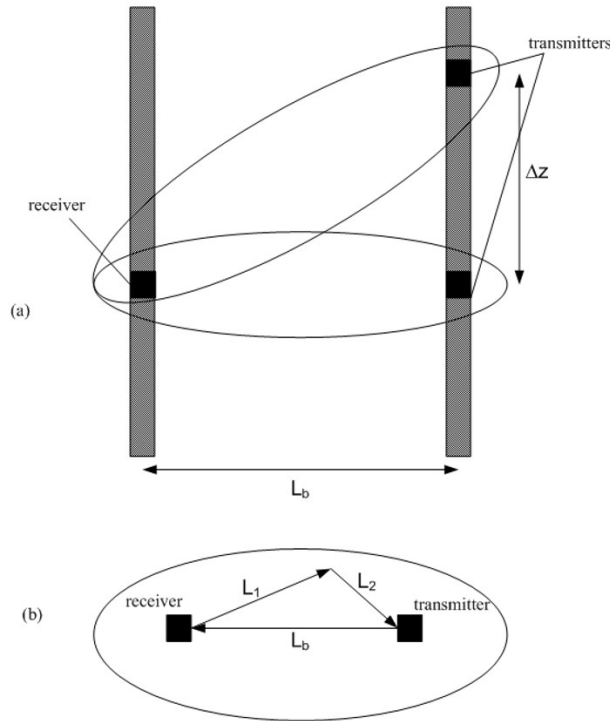


Figure 2. Fresnel's ellipse criterion, after Fernandez & Santamarina (2002) and Santamarina & Fratta (1998): (a) intersection of two Fresnel's ellipses; (b) size of Fresnel's ellipse.

Based on the above, the criterion is that the minimum interval between each two successive transducers is $\lambda / 2$.

3.3 Resolution of travel time

The vertical separation between transducers Δz must be chosen so that the difference in travel time between one source and any two consecutive receivers, t_1 and t_2 (Figure 3), can be detected within the resolution in travel time measurement ϵ_t (Lee, 2003; Lee et al., 2005). This is expressed by Equations 9 to 11 as follows:

$$t_1 = \frac{L_b}{V_{med}} \quad (9)$$

$$t_2 = \frac{\sqrt{L_b^2 + \Delta z^2}}{V_{med}} \approx \frac{L_b}{V_{med}} \left[1 + \left(\frac{\Delta z}{L_b} \right)^2 \right] \quad (10)$$

$$\Delta z \geq \sqrt{L_b \cdot V_{med} \cdot \epsilon_t} \quad (11)$$

This criterion often imposes larger values of Δz than Fresnel's criterion. Therefore, it is very crucial to increase the resolution of travel time measurement (i.e. decreasing ϵ_t) in order to improve the tomographic resolution, ideally to a level where the Fresnel criterion governs.

4. Optimum vertical spacing and associated tomographic resolution

It is essential to check the highest achievable resolution in the tomographic experiment by checking the criteria explained in the previous section. To this end, the wavelength was considered for a medium with an average shear wave velocity of about 100-250 m/s, which is the range expected

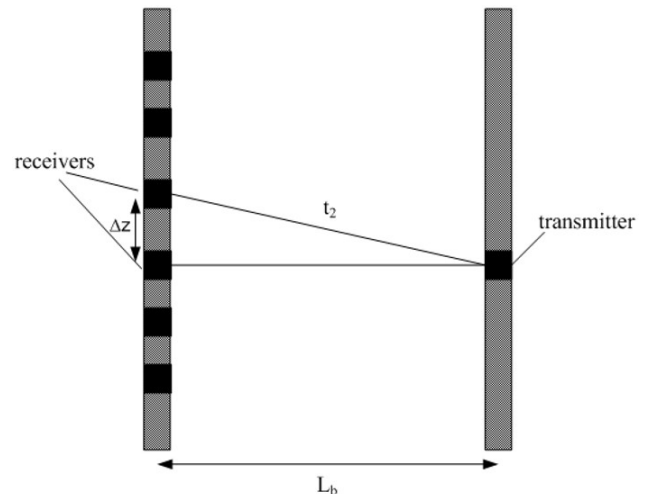


Figure 3. Resolution of travel time criterion.

for uncemented soils. This range of shear wave velocity was estimated using the power law relationship between shear wave velocity and the mean effective stress for silica sand at a range of stresses that will be imposed in a centrifuge model, given in Equation 12, where A is a factor depending on the soil properties:

$$V_s = A(\sigma')^m \quad (12)$$

The expected suitable frequency at this stress level will be about 10-20 kHz (from preliminary experimenting in the centrifuge). These values yield a wavelength of 0.5 – 2.5 cm. Checking against Fresnel's criterion, the separation between transducers Δz should not be less than $\lambda / 2$, which gives a Δz range of 0.25 – 1.25 cm. To check against the third criterion expressed in Equation 11, L_b was taken as 30 cm as the maximum value in a centrifuge model. The resolution of travel time measurement, ϵ_p , was taken as 2 μ s, which depends on the data acquisition system. Inserting these values into Equation 11 gives $\Delta z \geq 1.22$ cm.

Theoretically, based on the above analysis, an average resolution of about 1 cm for any cell dimension can be achieved. This will give a tomographic image with a cell size of 1 cm² in a 2-dimensional model or 1 cm³ for 3-D tomography. To achieve a resolution of 1 cm experimentally, the size of the transducers should be ≤ 1 cm. This study has made a breakthrough by reducing the spacing between the shear wave transducers to only 8 mm, as explained next.

5. Components of the ST system of the beam centrifuge at UWA

The ST system was developed for use with the beam centrifuge at UWA. The beam centrifuge is an Acutronic Model 661. It has a maximum payload of 400 kg at up to 100 g (≈ 1000 m/s²), decreasing to 200 kg at 200 g . The maximum radial distance between the cradle platform and the axis of rotation is 1.8 m. A full description of the beam centrifuge at UWA can be found in Fahey et al. (1990) and Randolph et al. (1991). The different components of the developed ST system are described in the following sections.

5.1 Bender element transducers

A basic description of the bender element can be found in many references (Dyvik & Madshus, 1985; Kuwano et al., 2000; Pennington et al., 2001; Lee & Santamarina, 2005; Leong et al., 2005). The most common piezoelectric ceramic used for bender elements is Lead Zirconate Titanate (PZT). There are different types of PZT: Shirley & Hampton (1978) used PZT4 bender elements; Brignoli et al. (1996) used PZT5A and PZT5HN bender elements, and Pennington et al. (2001) and Rammah et al. (2004) used PZT5B bender elements. In this study, the piezoceramic material type used for manufacturing

the bender elements is PZT5A supplied by Piezo Systems Inc. (PiezoSystemInc., 2005), USA. Two types of sheets were used: T220-A4-503X is X-poled for series connection, which was used for fabricating the receiver bender elements, and T220-A4-503Y is a Y-poled sheet with a parallel connection, which was used for the fabrication of the transmitter bender elements. The dimensions of these sheets are: width = 31.8 mm, length = 63.5 mm, and thickness = 0.51 mm.

5.2 Design and fabrication of a miniature bender element transducer

Initially, it was necessary to design one pair of prototype bender elements (one transducer and one receiver) that meets the requirements below:

- The benders must have a small size to meet the spacing requirement of the transducers and hence the desired resolution as discussed above.
- The benders must provide a range of frequencies that provides the wavelength necessary for the required resolution.
- The benders must be waterproof for use in moist conditions.
- Cross-talks must be eliminated by providing robust shielding.
- The bender elements must be sufficiently robust and reliable to withstand the relatively harsh environment of the centrifuge.

To achieve the above requirements, the following design criteria were addressed:

The diameter of the bender element socket was chosen to be 8 mm (outside diameter) to allow a spacing of 10 mm from centre to centre. Accordingly, the width of the bender element itself, b , had to be reduced to only 6 mm to fit the socket. The thickness of the bender element t , is 0.51 mm (for the PZT5A). These dimensions apply to both the transmitters and receivers.

The resonant frequency of a bender element in the air differs from the resonant frequency when it is embedded into the soil. Lee & Santamarina (2005) conducted both analytical and experimental studies to estimate the resonant frequency of bender elements in the air and the soil. The cantilever length (i.e. protrusion outside the socket) of a bender element, L_b , affects its resonant frequency in air and soil, its free deflection, the force generated by the transmitter, and the output voltage generated by the receiver. For the system presented here, a cantilever length, L_b , of 4 mm was chosen, which provides a theoretical resonant frequency of about 14.7 kHz. This resonant frequency lies within the range of frequencies required to achieve a resolution of 10 mm.

5.3 Fabrication of a miniature bender element

For the ST system with a resolution of 1 cm and model cross-section dimensions of 26 cm \times 26 cm, the number of

transducers needed for a cross-hole tomography configuration is 52 (26 transmitters and 26 receivers). For a three-sided illumination tomography setup, the number of transducers will be 78; one array contains 26 transmitters and two arrays, each containing 26 receivers. Based on that, there was a need for a large number of bender element transducers to be manufactured. The most effective way was to manufacture all bender elements in an assembly-line fashion. To achieve this, a procedure was developed to allow 16 bender elements to be coated simultaneously using a mould which was designed and made in the workshop at UWA. Prior to coating, a number of strips of 6 mm x 15 mm piezoelectric elements were cut and then coated simultaneously. Then each strip was connected to a water-proof well-shielded co-axial cable after allowing the epoxy to harden. Each coated strip was placed in the centre of a stainless-steel cylindrical socket, 8 mm outer diameter and 20 mm long, with the bender element protruding 4 mm beyond the end of the socket. The sockets were filled under a vacuum with epoxy resin to ensure that the bender element behaves as a fixed-ended cantilever. Figure 4 shows a schematic diagram of the produced bender element.

5.4 Checking time delay in tip-to-tip contact

To illustrate the time delay caused by the electronic components and coating material, the transmitter and receiver were brought into tip-to-tip contact. Then both transmitted and received signals were recorded. A time delay of 12 μ s was monitored when the bender elements were brought to tip-to-tip contact. In all cases, this time delay value was subtracted from the measured arrival time for the calculation of shear wave velocity.

5.5 Measuring the resonance frequency of bender elements

The resonance frequency of the bender elements was measured by bringing a transmitter and a receiver into tip-to-tip contact. Then a series of sine waves of a frequency of 1 kHz to 100 kHz were sent, and the receiver response was monitored by the oscilloscope. The peak-to-peak amplitude of the received signal was measured for each value of the input frequency input. The resonance frequency in the air is the value that produced the highest response from the receiver in terms of voltage. The obtained resonance frequency was \approx 10 kHz.

6. Tomographic frame for holding transducers

The tomographic frame for a centrifuge seismic tomography had to be designed to:

- hold the bender element transducers while providing a small gap (2 mm) of isolating material between any two successive transducers;

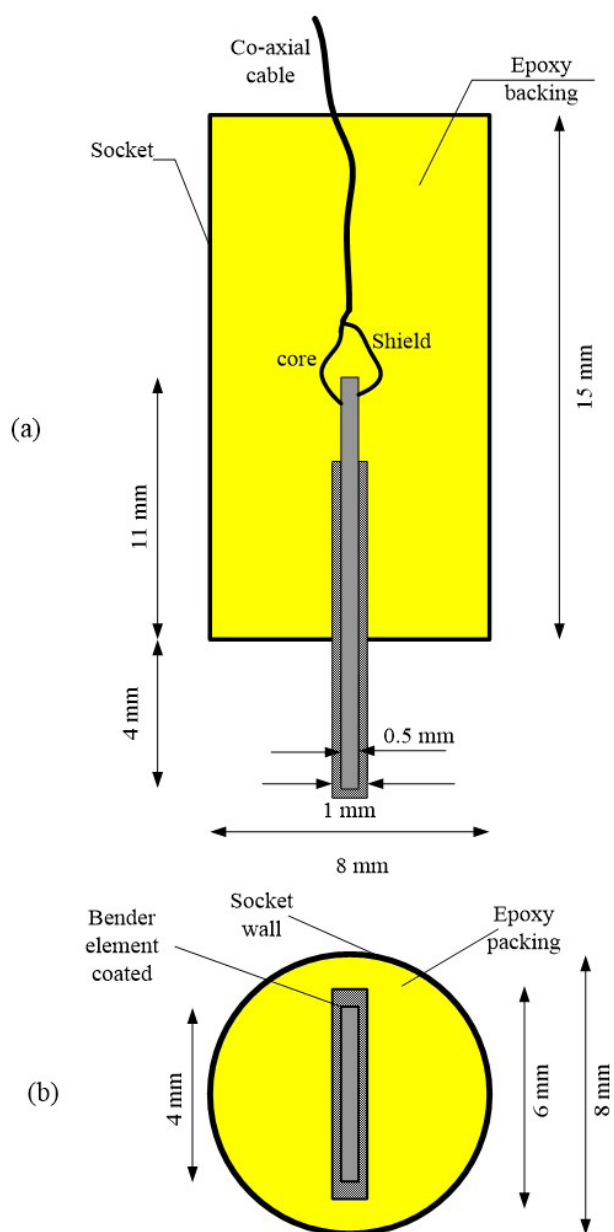


Figure 4. Bender element produced at UWA: (a) side elevation (b) front view of the bender element transducer.

- prevent the vibration that may be transmitted from any activated bender element through the frame body;
- provide proper electrical shielding for the bender element body to reduce the electrical noise and eliminate any possible cross-talk;
- prevent any reflections of compression waves due to the transverse directivity nature of the bender elements; some of these challenges have been discussed in (Lee et al., 2005) and (Lee, 2003).

Different configurations and materials were tried in designing a frame to meet the above requirements; eventually, relatively stiff rubber strips (300 mm long by 25 mm wide by

20 mm thick) were used as frames. Holes of 8 mm diameter and 10 mm centre-to-centre spacing were carefully drilled along the rubber strip, and the bender elements were pushed into these holes. Figure 5 shows part of the array.

To provide robust electrical shielding, all bender element casings were connected using a thin conductive wire, which eventually was connected to the centrifuge electrical earthing system. Three identical strips were prepared, each capable of accommodating up to 30 bender elements.

The reason for using separate holders (strips) was to avoid any possibility of cross-talk between transmitters and receivers through the holder and to have flexibility in setting the spacing between transmitters and receivers in the model. Figure 6 shows a schematic diagram of the arrangement of the frames within a centrifuge box.

The advantage of using three-sided illumination (i.e. bender arrangement) (Figure 6) is to improve the ray coverage and hence improve the quality of a tomographic image. If needed in the future, further improvement of ray coverage can be achieved by adding a similar array of either transmitters or receivers at the top of the soil model.



Figure 5. Array of bender elements mounted on a tomographic frame.

7. High voltage amplifiers and multiplexing system

The configuration of the tomographic model in Figure 6 consisted of 26 transmitters in the left-hand vertical array and 52 receivers (26 in the right-hand vertical array and 26 in the array at the bottom). A tomographic experiment requires scanning a medium by sending waves from all transmitters to all receivers. This implies that, during centrifuge testing, a system is required to provide the ability to switch through all transmitters and receivers whilst the centrifuge is spinning. To achieve this, a reliable and robust hardware system with the capability of accommodating such a large number of transducers was designed and built in the electronic workshop at UWA.

7.1. High voltage piezo driver

Four high-voltage amplifiers (HVA) boxes were manufactured. Each box has a capacity of 16 channels, giving a total capacity of 64 channels, which can be connected to 64 transmitters. Each channel on any specific HVA box can be addressed digitally by a Binary Coded Decimal (BCD) code written as a subroutine in the data acquisition software. Strong cases that withstand centrifugal forces were used to house the boards in flight.

7.2 Piezo receiver amplifiers

Six amplifier boxes, each with a capacity of 10 channels, were manufactured. Each channel can be addressed digitally using a second Binary Coded Decimal (BCD) code written in the data acquisition software. The amplification factor was set to $\times 100$ for the received signal.

8. Data acquisition system for tomographic scanning

A National Instruments data acquisition card (NI PCI-6251 – M-series - 16 bit) with a 1.2 Mega sample per second sampling rate. The sampling rate is a key parameter for acquiring and receiving signals driven at a high frequency, such as the 20 kHz used in this development.

An efficient data acquisition software was written in *Labview 7.1* with the following features:

- The parameters of the transmitted signal can be specified in terms of amplitude, waveform, frequency, sampling rate and delay time between successive transmitted signals. In addition, the waveform can be chosen to be a sine wave or a step or pulse function.
- The desired bender element transmitter can be chosen by selecting its channel number (1 to 64). The required channel in the high-voltage amplifier is addressed digitally by the BCD.

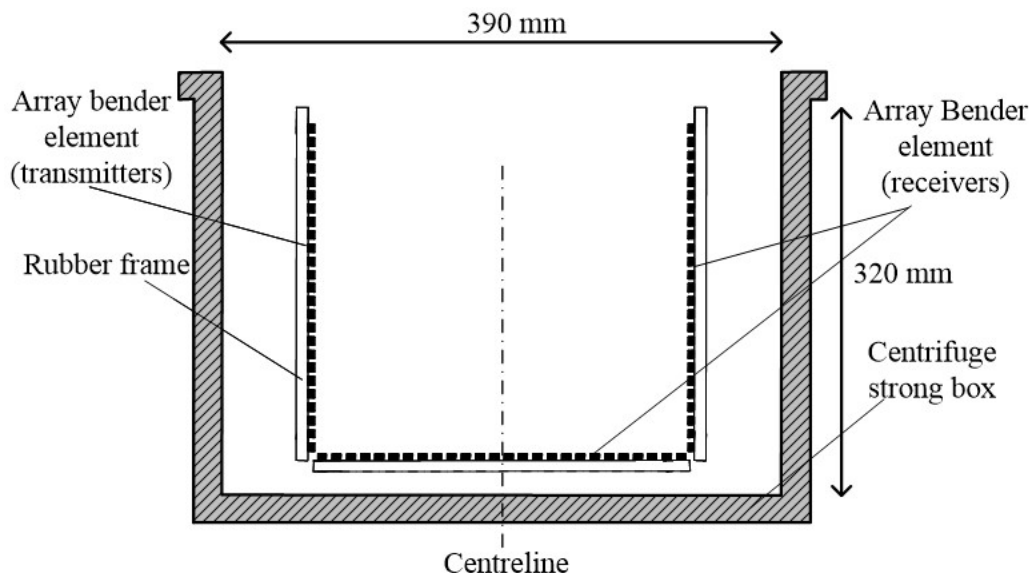


Figure 6. Tomographic model in centrifuge box (3-side illumination).

- The desired bender element receiver can be activated by selecting its channel number (1 to 60), also by the BCD.
- Both transmitted and received signals are displayed on the screen, with cursors to allow manual measurement of the travel time.
- Records of both transmitted and received signals are saved in both ASCII and binary formats.
- An option for stacking signals (averaging) is provided. This is crucial for increasing the signal-to-noise ratio, especially in the centrifuge, where considerable mechanical and electrical noise is expected.
- The software allows automatic scanning by specifying the initial and final channel numbers for transmitters and receivers. For example, in the model shown in Figure 6 with 26 transmitters and 52 receivers, if complete tomographic scanning is required, the program generates a signal from transmitter #1 to all 52 receivers, starting from # 1 up to #52. Then it repeats the same for transmitter #2 until it covers all possible combinations. This leads to a large number of signals (1352 signals in this particular case). All these records are stored on the hard drive of the computer.

9. Picking the arrival times of shear waves in a tomographic experiment

The number of measurements (signals) for the three-sided illumination is 1326; this can reach 2500 measurements if an additional array of transmitters is installed at the top of the centrifuge model. This large number requires both practical and efficient methods to pick the shear wave's first

arrival. Therefore, it was decided to use **Promax 2D** software. This software enables both automatic and manual picking of arrival time, and it also has a complete library of signal processing routines, including different types of filtering.

9.1 Tomographic inversion

It should be noted that for the case where straight ray tomography is considered, the matrix of travel lengths L is independent of the slowness model S . In this case, L can simply be obtained from the model's geometry and locations of sources and receivers. However, in nonlinear tomography, L becomes an implicit function of S . Therefore, in this case, a ray-tracing technique should be applied to define the ray path through the slowness model.

In linear tomography, L and T are given, and the objective is to determine the slowness model S . The assumption here is that the ray paths are known *a priori*, which is justified by a linear approximation, which ignores the ray paths' dependence on the slowness distribution. Typically, the ray paths are assumed to be straight lines connecting sources and receivers.

In nonlinear tomography, the only given information is the vector of measured travel time T , along with data acquisition geometry (the coordinates of all sources and receivers). Therefore, the non-linear tomographic inversion aims to determine the slowness model S . The nonlinear inversion is an iterative process that starts with the computation of the initial S model. First, a forward ray-tracing process is performed on the initial S to obtain L , hence the computed travel time. The difference between the measured and computed travel time is then calculated. In the next iteration step, the S model is updated. The iteration process continues until the

difference between the measured and computed travel time vectors is sufficiently small.

In nonlinear problems, the dependence of the ray paths on the slowness distribution of the medium strongly influences the design of the inversion algorithm. Therefore, nonlinear inversion is required for problems with significant slowness variation across the medium. For such media, the ray paths normally show large curvature (i.e., nonlinear), which cannot be known before the inversion process begins.

Both linear and nonlinear tomographic inversions were applied to the travel-time data obtained from the different tests to recover the V_s models. The linear tomographic inversion assumes that the rays are straight. In a nonlinear inversion, the rays were traced using the eikonal method. In general, the tomographic inversion is highly dependent on the ray coverage. It has been shown that by increasing the ray coverage, the solution becomes more stable, the resulting images become better, and the error decreases (Woodward et al., 2008).

There is no unique solution in tomography because of the uneven ray coverage. Therefore, adding constraints or *a priori* information to the solution system is essential. This is usually achieved by implementing regularisation approaches. There are no unique guidelines for selecting the different regularisation factors. However, optimal values for these factors should be selected in order to meet two criteria: 1) the output model is physically meaningful; 2) the resulting model conforms as closely as possible to the measured travel time data by minimising the residuals in travel-time data.

The tomographic inversion results carried out on travel-time data from both 1g and centrifuge tests are presented in the following sections.

9.2 Tomographic experiment using the ST system on a homogeneous-isotropic wax block at 1g

Before performing centrifuge tests using the ST system, it was decided to carry out a seismic tomography test at 1g on a model with a known shear-wave velocity. The test aimed to calibrate and verify the performance of the ST system, including hardware, data acquisition software, and inversion codes. For this purpose, a wax block with dimensions of $269 \times 280 \times 200$ mm was prepared. A cube of wax with an edge dimension of 269 mm was prepared by pouring molten wax into a mould and allowing it to harden. A dimension of 269 mm was chosen in order to avoid near-field effects. Moreover, increasing the travel distance was also desirable to reduce the impact of any error associated with determining the arrival time in the high-shear-wave-velocity wax. Therefore, the bender elements were embedded on two opposite ends of the wax block, such that the tip-to-tip travel distance was 260 mm.

In order to embed the two arrays of receivers and transmitters, a channel with a width of 1.5 mm and a depth of 4.5 mm was made on two opposite sides (the sides with

the dimension of 280×200 mm) of the already hardened wax block. These dimensions were chosen to be slightly bigger than the dimensions of the bender elements, which are 4×1 mm. In order to ensure a good coupling between the bender elements and the wax block, the molten wax was poured into the channel, and one array was inserted immediately before the wax in the channel hardened. The same was repeated for installing the other array of bender elements.

Ideally, the wax block is supposed to be both homogeneous and isotropic; therefore, it was decided to use linear tomographic inversion as a first choice. The output tomogram resulting from inverting the travel-time data is shown in Figure 7. For the purpose of evaluating the inverted tomogram, a homogenous model with $V_s = 960$ m/s was considered to be the exact model. The resulting V_s tomogram of the wax block indicates a maximum relative difference of 14% compared to the “theoretical” wax model with $V_s = 960$ m/s. Therefore, the measured data set collected on the wax block was inverted using nonlinear tomography based on the eikonal method (Rammah, 2008).

In the case of a homogeneous model, both linear and nonlinear tomography gave similar results, i.e., either method can be used for the inversion. Therefore, any deviation from a homogenous model exhibited by the tomogram could be due to 1) that the wax block is not 100% homogenous, i.e., ideal homogeneity could not be achieved during the sample preparation and hardening; 2) certain error and randomness in picking the first arrival of shear waves could have yielded an error, i.e., miss picking the first arrival by a small value would yield a significant error, especially for such fast shear wave travel times (travel time ranges between 270 μ s and 480 μ s).

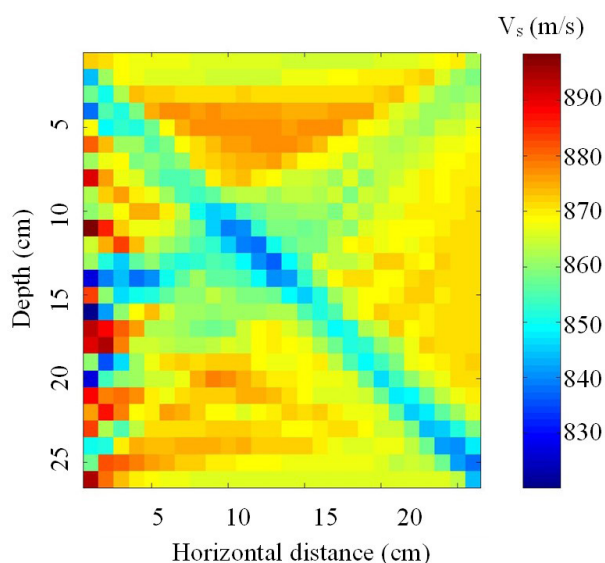


Figure 7. Output tomogram of shear wave velocity obtained from straight-ray tomographic inversion of travel-time data obtained on the wax block.

9.3 Tomographic experiments using the ST system in a centrifuge model

Four centrifuge tests were carried out on models with overburden stresses resulting from the self-weight stress of the silica sand used in the models. The seismic tomography centrifuge model was prepared by the dry pluviation method using a ‘travelling sand curtain’ hopper. After placing a 20 mm layer of fine silica sand in the base of the centrifuge box (to prevent possible crosstalk between the tomographic frame and the strongbox), the seismic tomography frames were installed in the desired position using temporary clamps attached to the box (Figure 8). The horizontal distance between the two vertical arrays of bender elements was 260 mm. The sand was rained from a constant height of 1.20 m, with a curtain travel speed of 120 mm/s. The drop height was adjusted every 10 mm to ensure the homogeneity of the sand. The resulting relative density (D_r) was 95%, the void ratio (e) was 0.50, and the dry unit weight (γ_d) was 17.8 kN/m³.

To confirm the absence of mechanical crosstalk either through the frames themselves or the centrifuge box, the sand hopper was stopped when the centrifuge box had been filled to mid-height. Then the clamps shown in Figure 8 were removed, and several shear wave measurements were taken between one of the buried transmitters and the unburied receivers.

No signal was detected by any of these receivers, confirming the absence of mechanical crosstalk. The sand-raining procedure was resumed until the two vertical arrays of bender elements were embedded into the soil. Finally, the two clamps were removed, and the box was mounted on the centrifuge platform.

Four centrifuge tests were carried out at 50, 100, 150 and 200g. In each test, a complete tomographic scan was performed. For the tests at 50 and 100g, the input signal consisted of a single 10 kHz sine wave, repeated 20 times, with the outputs stacked to obtain a single output signal. However, the frequency was increased to 15 kHz for the tests at 150 and 200g, repeated 30 times due to a higher noise level at these higher g-levels.

Figure 9 shows a typical shear wave signal from the centrifuge test at 200g. This signal is for transmitter and receiver pair located at a depth of 130 mm under the soil surface. This depth is equivalent to 26 m at the prototype scale, with an effective vertical stress of 463 kPa. The high signal-to-noise ratio in this (after stacking 30 signals) signal can be noted in Figure 9.

The first arrivals of the shear waves gathered in the above tests were picked using Promax. Figure 10a shows the horizon of the first arrival of the common-source signal for transmitter # 9. Next, the first arrivals of all 1352 signals were plotted in the form of a map, as shown in Figure 10b. Unlike the wax block model, where the rays were straight lines due to the homogeneity of the model, the seismic rays propagating through the silica sand model in the centrifuge are expected to curve due to the nonlinearity of the soil

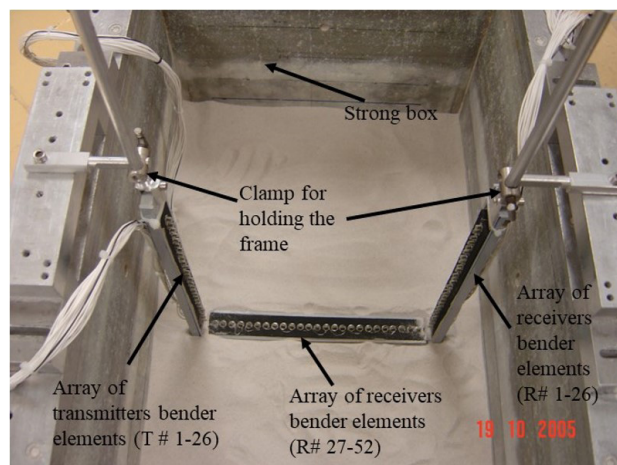


Figure 8. Tomographic model in centrifuge box prior to sand raining.

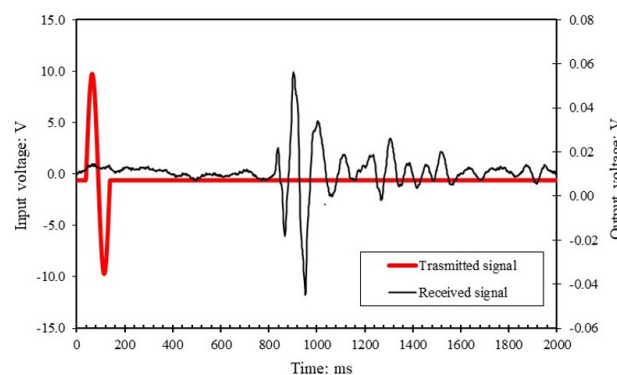


Figure 9. Improved shear wave measurement on silica sand at 200g at a depth of 13 cm: shear wave between transmitter # 13 and receiver # 13.

stiffness resulting from the nonlinearity of the variation of stresses over the depth of the sand layer. This was illustrated by carrying out forward modelling in which the seismic rays were traced through a model equivalent to the silica sand model tested at 100g. The relationship in Equation 12 was used to derive the V_s model. Figure 11a shows the model in the background and the family rays for source #2, which were traced using the eikonal method.

It can be seen that the rays are indeed curved, and the curvature is evident in the top part of the model. Therefore, it is clear that the imposition of a straight-ray assumption in the inversion process would not be the proper choice in this case. Thus, the travel-time data sets obtained from the silica sand models in the centrifuge were inverted using nonlinear tomography based on the eikonal method for tracing the rays. Figure 11b shows an interpolated output tomogram obtained by inverting the data from the test at 100g, which was acquired by applying a regularisation approach that adds smoothing in the horizontal direction. The regularisation coefficient for the horizontal smoothening was used to minimise the root-mean-squares of

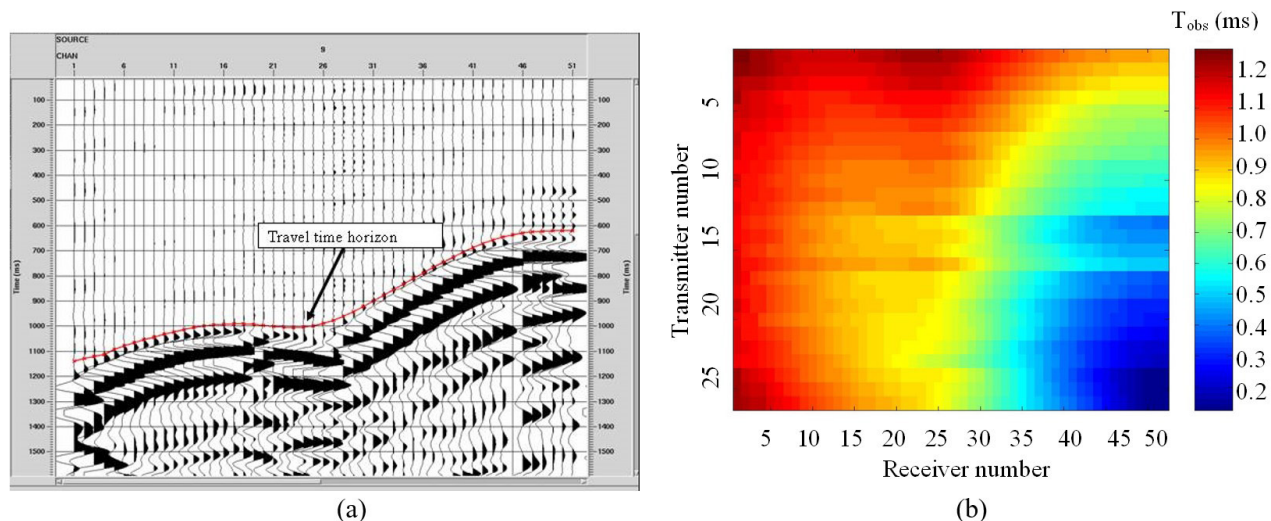


Figure 10. First arrivals of shear wave signals obtained from the centrifuge test on silica sand at 100g: (a) results from the Promax program for common source shots – transmitter # 9 shots; (b) map of observed first arrivals of shear waves.

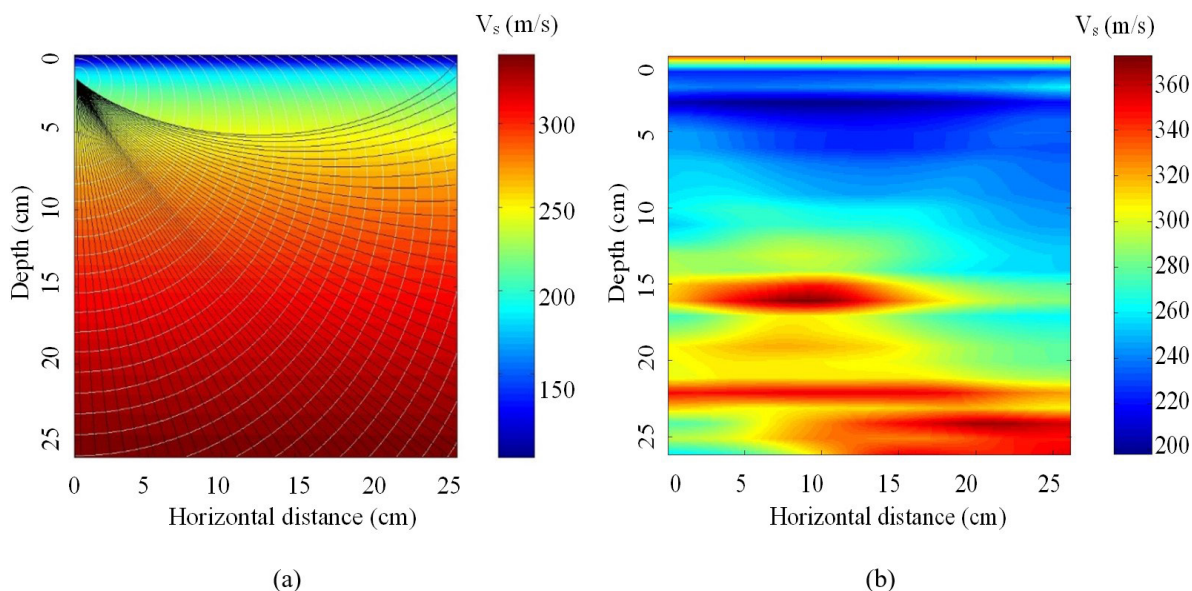


Figure 11. Nonlinear tomographic inversion of travel-time data obtained from the centrifuge test on silica sand at 100g: (a) forward modelling by tracing the rays using the eikonal method on an equivalent isotropic V_s model due to overburden stresses at 100g - family rays and wavefronts for source# 2; (b) interpolated output tomogram of V_s .

residuals of the travel-time data. As expected, the tomogram of V_s presented in Figure 11b indicates increasing values of V_s with depth. In addition, some lenses of higher values of V_s (anomalies) can be observed, such as those at an approximate depth of 15 cm, which might be attributed to a high density of sand.

10. Conclusions

This paper described the development of a high-resolution seismic tomography (ST) system for the beam centrifuge at UWA. The paper documents the different components of the

system, including bender element transducers, tomographic frame, high-voltage piezo drivers and data acquisition software. Design criteria that affect the determination of the resolution of the tomographic image were discussed.

The ST system was calibrated at 1g using a block of wax with a known shear-wave velocity. A homogenous V_s model of the wax block was recovered properly by inverting the travel-time data using linear tomography based on the assumption of straight rays.

The ST system was used on a silica sand model subjected to self-weight stresses in the geotechnical centrifuge at

a 100g level. Tomographic inversion was carried out on the measured travel time data obtained from these tests. Forward modelling carried out on a theoretical V_s model resembling the silica sand model in the centrifuge showed that the seismic rays are curved due to the nonlinearity of the soil over the soil depth. Therefore, nonlinear inversion was performed on the travel-time data to recover the V_s models in the centrifuge. The resulting V_s obtained at 100g resembled the expected variation of V_s . The results of the inversion and the rays traced during the inversion process confirm the nonlinearity of the rays in the tested soil in the centrifuge.

The overall results obtained from applying the ST system at both 1 g and the centrifuge demonstrated that the ST system is a promising tool for imaging V_s models involved in different geotechnical problems. However, studies carried out on both synthetic, 1g and 100g centrifuge models showed that, in most cases, there are some limitations with regard to the limited ray coverage and the dependency of the inversion on *a priori* information. Nevertheless, increasing the ray coverage from 3-sided to 4-sided by adding a fourth array at the surface can improve the ray coverage, particularly for the nonlinear soil model tested in the centrifuge.

Acknowledgements

The authors would like to acknowledge the Centre for Offshore Foundation Systems (COFS) and the School of Civil Engineering at the University of Western Australia (UWA) for their generous financial support and interest in this study. The first author held a University Postgraduate Award (UPA) at the time of this study.

Declaration of interest

The authors have no conflicts of interest to declare. All co-authors have observed and affirmed the contents of the paper, and there is no financial interest to report.

Authors' contributions

Khader Ibrahim Rammah: conceptualization, investigation, methodology, formal analysis, software, writing – original draft, writing – review & editing. Mostafa Ali Ismail: conceptualization. Jesse Costa: software. Mario Vicente Riccio Filho: writing – review & editing.

Data availability

Data generated and analyzed in the course of the current study are not publicly available due to data ownership, but a complete or limited dataset can be made available by the corresponding author upon reasonable request.

List of symbols and abbreviations

| | |
|-----------------|--|
| BCD | Binary Coded Decimal |
| e | void ratio |
| f | Wave frequency |
| G_0 | small strain stiffness |
| H | height of a tomographic model |
| HVA | High-Voltage Amplifiers |
| L | array travel distances |
| $[L]$ | matrix of travel lengths |
| L_b | distance between arrays of transmitters and receivers in a cross-hole tomography |
| m | number of measurements in a tomographic experiment |
| N_p | number of nodes in a tomographic mesh |
| PZT | Lead Zirconate Titanate (Piezoceramic) |
| S | slowness of seismic ray |
| $[S]$ | slowness vector for all pixels in the mesh of the tomographic model |
| ST | Seismic Tomography |
| t | travel time of a seismic ray |
| $[T]$ | vector of travel time in a tomographic model |
| V | phase velocity of a wave |
| V_s | Shear wave velocity |
| γ_d | dry unit weight |
| Δz | vertical separation distance between transducers in a tomographic model |
| ε_t | Resolution of travel time measurement |
| λ | wavelength |

References

- Berryman, J.G. (1991). *Lectures notes on nonlinear inversion and tomography*. University of California.
- Brignoli, E.G.M., Gotti, M., & Stokoe, K.H.I. (1996). Measurement of shear waves in laboratory specimens by means of piezoelectric transducers. *Geotechnical Testing Journal*, 35(6), 1032-1040.
- Dyvik, R., & Madshus, C. (1985). Lab measurements of G_{max} using bender elements. In *Proceedings of the Conference on Advances in the Art of Testing Soils Under Cyclic Conditions* (pp. 186-196). Detroit, MI.
- Fahey, M., Finnie, I., Hensley, P.J., Jewell, R.J., Randolph, M.F., Stewart, D.P., Stone, K.J.L., Toh, S.H., & Windsor, C.S. (1990). *Geotechnical centrifuge modelling at the University of Western Australia* (Report No: Geo:90092). The Department of Civil Engineering, The University of Western Australia.
- Fernandez, A., & Santamarina, J.C. (2002). Design criteria of geotomographic field studies. *Geotechnical Testing Journal*, 26(4), 410-420.
- Fu, L., Zeng, X., & Figueroa, L. (2004). Shear wave measurement in centrifuge using bender elements. *International Journal of Physical Modelling in Geotechnics*, 4(2), 01-11. <https://doi.org/10.1680/ijpmg.2004.040201>.

- Ismail, M.A., & Hourani, Y. (2003). An innovative facility to measure shear-wave velocity in centrifuge and 1-g models, deformation Characteristics of Geomaterials. In *Proceedings of the 3th International Symposium ISLyon* (pp. 21-29). A.A. Balkema Publishers.
- Kita, K., Shibata, T., Yashima, A., & Kobayashi, S. (1992). Measurement of shear wave velocities of sand in a centrifuge. *Soil and Foundation*, 32(2), 134-140. <http://dx.doi.org/10.1520/GTJ20130189>.
- Kuwano, R., Connolly, T.M., & Jardine, R.J. (2000). An isotropic stiffness measurements in a stress-path triaxial cell. *ASTM Geotechnical Testing*, 23(2), 141-157. <http://dx.doi.org/10.1520/GTJ11039J>.
- Lee, J.-S. (2003). *High resolution geophysical techniques for small-scale soil model testing* [Doctoral thesis, Georgia Institute of Technology]. Georgia Institute of Technology's repository. Retrieved in January 23, 2022, from <http://hdl.handle.net/1853/5329>
- Lee, J.-S., & Santamarina, J.C. (2005). Bender elements: performance and signal interpretation. *Journal of Geotechnical and Geoenvironmental Engineering*, 131(9), 1063-1070. [http://dx.doi.org/10.1061/\(ASCE\)1090-0241\(2005\)131:9\(1063\)](http://dx.doi.org/10.1061/(ASCE)1090-0241(2005)131:9(1063)).
- Lee, J.-S., Fernandez, A., & Santamarina, J.C. (2005). S-Wave velocity tomography: small-scale laboratory application. *Geotechnical Testing Journal*, 28(4), 336-344.
- Leong, E.C., Yeo, S.H., & Rahardjo, H. (2005). Measuring shear wave velocity using bender elements. *Geotechnical Testing Journal*, 28(5), 329-342. <http://dx.doi.org/10.1016/j.sandf.2015.02.009>.
- Menke, W. (1984). *Geophysical data analysis: discrete inverse theory*. Academic Press.
- Nolet, G. (1987). *Seismic tomography with application in global seismology and exploration geophysics*. Springer.
- Pennington, D.S., Nash, D.F.T., & Lings, M. (2001). Horizontally mounted bender element for measuring anisotropic shear moduli in triaxial clay specimens. *Geotechnical Testing Journal*, 24(2), 133-144. Retrieved in January 23, 2022, from <https://www.astm.org/gtj11333j.html>
- PiezoSystemInc. (2005). *Piezoelectric Sheets & Plates*. Piezo. Retrieved in January 23, 2022, from <http://www.piezo.com/>
- Rammah, K.I. (2008). *Development of a seismic tomography system for use on a geotechnical centrifuge* (Doctoral thesis, The University of Western Australia). The University of Western Australia's repository. Retrieved in January 23, 2022, from <https://research-repository.uwa.edu.au/en/publications/development-of-a-seismic-tomography-system-for-use-on-a-geotechni>
- Rammah, K.I., Ismail, M.A., & Fahey, M. (2006). Development of a centrifuge seismic tomography system at UWA. In *Proceedings of the 6th International Conference on Physical Modelling in Geotechnics* (Vol. 1, pp. 229-234). Hong-Kong.
- Rammah, K.I., Val, D.V., & Puzrin, A.M. (2004). Effects of ageing on small-strain stiffness of overconsolidated clays. *Geotechnique*, 54(5), 319-322. <http://dx.doi.org/10.1680/geot.2004.54.5.319>.
- Randolph, M.F., Jewell, R.J., Stone, K.J.L., & Brown, T.A. (1991). Establishing a new centrifuge facility. In: *Proceedings of the International Conference Centrifuge 91* (pp. 3-9). Boulder.
- Santamarina, J.C., & Fratta, D. (1998). *Introduction to discrete signals and inverse problems in civil engineering*. The American Society of Civil Engineers (ASCE).
- Shirley, D.J., & Hampton, L.D. (1978). Shear-wave measurements in laboratory sediments. *The Journal of the Acoustical Society of America*, 63(2), 607-612. <https://doi.org/10.1121/1.381760>.
- Woodward, M.J., Nichols, D., Zdraveva, O., Whitfield, P., & Johns, T. (2008). A decade of tomography. *Geophysics*, 73(5), VE5. <http://dx.doi.org/10.1190/1.2969907>.
- Young, J.M., Sanchez-Salinerio, I., Stokoe, K.H., & Roesset, J.M. (1988). In situ damping measurements by crosshole seismic method. In J.M. Joug. *Earthquake Engineering and Soil Dynamics II—Recent Advances in Ground-Motion Evaluation* (pp. 305-320). American Society of Civil Engineers.